PHYSICAL REVIEW B **80**, 081402(R) (2009)

Fermi energy dependence of the *G*-band resonance Raman spectra of single-wall carbon nanotubes

J. S. Park,[1] K. Sasaki,[2] R. Saito,[1] W. Izumida,[1] M. Kalbac,[3] H. Farhat,[4] G. Dresselhaus,[5] and M. S. Dresselhaus[6,7]
[1]*Department of Physics, Tohoku University and CREST, Sendai 980-8578, Japan*
[2]*National Institute for Material Science, Tsukuba 305-0044, Japan*
[3]*J. Heyrovsky Institute of Physical Chemistry, Academy of Sciences of the Czech Republic, CZ-18223 Prague 8, Czech Republic*
[4]*Department of Materials Science and Engineering, Massachusetts Institute of Technology, Cambridge, Massachusetts 02139-4307, USA*
[5]*Francis Bitter Magnet Laboratory, Massachusetts Institute of Technology, Cambridge, Massachusetts 02139-4307, USA*
[6]*Department of Electrical Engineering and Computer Science, Massachusetts Institute of Technology, Cambridge, Massachusetts 02139-4307, USA*
[7]*Department of Physics, Massachusetts Institute of Technology, Cambridge, Massachusetts 02139-4307, USA*
(Received 29 May 2009; published 4 August 2009)

The Fermi energy dependence of the *G*-band resonance Raman spectra of single-wall carbon nanotubes (SWNTs) is calculated, including the Kohn anomaly effect for metallic tubes. The gate voltage dependence of the *G*-band Raman spectra for SWNTs shows chirality-dependent G^+/G^- spectra, reflecting their dependence on the eigenvector direction of the optical (LO and TO) phonon modes and the nanotube chirality.

DOI: 10.1103/PhysRevB.80.081402 PACS number(s): 78.67.−n, 73.63.Fg

The *G*-band Raman spectra of single-wall carbon nanotubes (SWNTs) arise from the first-order, one-phonon, and intravalley *G*-band Raman-scattering processes,[1,2] which have been widely utilized for characterizing SWNTs and graphene. The *G*-band spectra of a SWNT consist of a higher-frequency peak (G^+) near 1580∼1590 cm^{-1} and a lower-frequency peak (G^-) in the range 1550∼1570 cm^{-1}. For semiconducting tubes (S-SWNT), the G^+ and G^- peaks can be assigned to longitudinal-optical (LO) and transverse-optical (TO) phonon modes, respectively, while the G^+ and G^- peaks of metallic tubes (M-SWNTs) are assigned to TO and LO phonon modes, respectively, because of the Kohn anomaly (KA) effect for phonons at the Γ point.[3–8] For the KA effect, the self-energy correction to the LO and TO phonon modes by the virtual excitation of an electron-hole pair causes a softening and a hardening of the LO and TO phonon frequencies, respectively.[7–9]

Recently Nguyen *et al.*[7] and Farhat *et al.*[8] observed the Fermi energy (E_F) dependence of the phonon-softening effect of SWNTs by using an electrochemical gate, and their results clearly show that the LO phonon mode softens as a function of E_F. Thus the E_F-dependent Raman spectra measurement is important for SWNT field effect transistor operation. However, the observed *G*-band Raman spectra of an individual SWNT show an anomalous behavior depending on the chirality (n,m) of a SWNT,[10] caused in part by the dependence of the relative intensity of the Raman G^+ to G^--band features (I_{G^+}/I_{G^-}) on the chirality and diameter.[11] For S-SWNTs, the G^+ peak is dominant at the zigzag chiral angle (θ=0°), while both the G^+ and G^- peaks appear at other chiral angles ($0° < \theta < 30°$). It has been known that the **k**-dependent electron-phonon (el-ph) interaction gives rise to the chirality dependence of both the *G*-band (Refs. 9 and 12) and radial breathing mode (RBM) (Ref. 12) Raman intensities. Thus the *G*-band spectral analysis is still not well understood, even though the *G* band has been studied for many years. In this Rapid Communication, resonance Raman spectra of SWNTs as a function of E_F are calculated in order to understand and interpret the chirality and E_F-dependent *G*-band spectra. We show here that the **k**-dependent el-ph interaction affects both the I_{G^+}/I_{G^-} relative Raman intensity and their spectral widths.

The self-energy corrections to the *G*-band phonon frequencies due to the KA affect not only the LO mode but also the TO mode, and both the LO and TO phonon frequencies depend on the chiral angle θ. The *G*-band Raman intensity *I* is calculated as a function of phonon energy $\hbar\omega$ and laser excitation energy E_L by[1,13]

$$I(\omega, E_L) = \sum_j \left| \sum_{a,b} \frac{\mathcal{M}_{op}(j,b)\mathcal{M}_{ep}(b,a)\mathcal{M}_{op}(a,j)}{\Delta E_{aj}(\Delta E_{bj} - \hbar\omega)} \right|^2 \quad (1)$$

in which $\Delta E_{aj} \equiv E_L - (E_a - E_j) - i\gamma$, while *j*, *a*, and *b*, respectively, denote an initial state in the valence band, an excited state in the conduction band, and a scattered state for an excited electron. The electron-photon matrix elements ($\mathcal{M}_{op}$) (Refs. 14 and 15) and the el-ph matrix elements ($\mathcal{M}_{ep}$) (Ref. 12) are calculated by the extended tight-binding (ETB) model.[16,17] Here γ is defined by an energy full width half maximum (FWHM) of the Raman excitation profile, also called the resonance window.[18] γ is calculated by the uncertainty relation between γ and the lifetime τ of a photoexcited carrier, which depends on the SWNT diameter d_t and θ by experiment.[18] The dominant lifetime of a photoexcited electron in the conduction band is determined by fast phonon emission processes for all phonons that have nonzero matrix elements $\mathcal{M}_{ep}$ and γ is given by the Fermi golden rule.[18] Thus γ is written as

$$\gamma = 2\pi \sum_\nu \sum_f |\langle f|\mathcal{H}_{ep}|a\rangle|^2 \delta(E_f - E_a \pm \hbar\omega_\nu), \quad (2)$$

where each term in the summation taken over the final state $\langle f|$ indicates the transition probability per unit of time from an initial photoexcited state $|a\rangle$ to $\langle f|$. The delta function $\delta(E_f - E_a \pm \hbar\omega_\nu)$ expresses the energy-momentum conservation in the phonon emission and absorption processes, and

$\langle f|\mathcal{H}_{ep}|a\rangle$ indicates the el-ph interaction matrix element for 24 possible phonon-scattering processes.[12]

The phonon frequency ω of the LO and TO phonon modes at the Γ point for M-SWNTs is calculated by including the KA effect. The phonon energy $\hbar\omega$ becomes $\hbar\omega = \hbar\omega^{(0)} + \hbar\omega^{(2)}$, where $\omega^{(0)}$ is the original phonon frequency without the el-ph interaction, and $\omega^{(2)}$ is the quantum correction to $\omega^{(0)}$, which is given by[9]

$$\hbar\omega^{(2)} = 2\sum_{\mathbf{k}} \frac{|\langle eh(\mathbf{k})|\mathcal{H}_{ep}|\omega^{(0)}\rangle|^2}{\hbar\omega^{(0)} - [E_e(\mathbf{k}) - E_h(\mathbf{k})] + i\Gamma} \times \{f[E_e(\mathbf{k}) - E_F] - f[E_h(\mathbf{k}) - E_F]\} \quad (3)$$

in which the factor 2 comes from spin degeneracy and $E_e(\mathbf{k})[E_h(\mathbf{k})]$ is an electron (hole) energy with wave vector $\mathbf{k}$, and $\langle eh(\mathbf{k})|\mathcal{H}_{ep}|\omega^{(0)}\rangle$ represents the el-ph matrix element for creating an electron-hole pair with $\mathbf{k}$ by the el-ph interaction $\mathcal{H}_{ep}$, and $f(E)$ is the Fermi distribution function. The G-band spectral width is given by the decay width Γ. We calculate Γ self-consistently by calculating $\Gamma = -\mathrm{Im}(\hbar\omega^{(2)})$.[9] It is noted that γ and Γ are different from each other, though the interactions of γ and Γ originate from the same $\mathcal{H}_{ep}$. γ originates from the lifetime of a photoexcited carrier, while Γ originates from the lifetime of the phonon. In the experiment, γ and Γ appear, respectively, in the Raman excitation profile and in the Raman spectrum.

Figure 1(a) shows the calculated resonance Raman spectra for the G band of type I S-SWNTs (Ref. 9) with family number $p = 2n+m = 28$. The (n,m) SWNTs with the same family number p have a similar diameter to one another. The E_L and γ [see Fig. 1(c)] are taken from E_{22}^S for each (n,m) SWNT. The chiral angle can vary from $\theta = 0°$ to $\theta \sim 30°$. The intensity of the G^- peak (TO) is always smaller than that of the G^+ peak (LO) because $\mathcal{M}_{ep}^{R,LO} > \mathcal{M}_{ep}^{R,TO}$, as shown in Fig. 1(b), in which the notation R indicates the Raman scattering. It is important to point out that the electron-phonon matrix elements for Raman and KA are different[9] since both initial and final states are different. In particular, the intensity of the G^- peak vanishes for a (14,0) SWNT since $\mathcal{M}_{ep}^{R,TO}$ for zigzag SWNTs is zero, as shown in Fig. 1(b). Here $\mathcal{M}_{ep}^{R}$ is calculated for the phonon amplitude at 300 K. These calculated G-band Raman spectra can be compared with previous experimental results, which show only one peak in the G-band spectra of (n,m) SWNTs with special chiral angles.[10] The observed (n,m) SWNT can be assigned as a zigzag SWNT by the calculation. In order to explain this, the el-ph matrix elements for the LO and TO phonons with $\mathbf{q}=0$ are given by[9]

$$\mathcal{M}_{ep}^{R,LO} \equiv \langle e(\mathbf{k}), \omega_{LO}|\mathcal{H}_{ep}|e(\mathbf{k})\rangle = gu\cos\Theta_R(\mathbf{k}),$$

$$\mathcal{M}_{ep}^{R,TO} \equiv \langle e(\mathbf{k}), \omega_{TO}|\mathcal{H}_{ep}|e(\mathbf{k})\rangle = -gu\sin\Theta_R(\mathbf{k}), \quad (4)$$

respectively, where g is the el-ph coupling constant, u is the phonon amplitude, and $\Theta_R(\mathbf{k})$ is defined by an angle between the $\mathbf{k}$ vector from the K point of the 2D Brillouin zone to the van Hove singular point, k_{ii}, and the circumferential direction vector, $\mathbf{K}_1$,[19] as shown in Fig. 1(e). Since $\Theta_R(\mathbf{k})$ is zero for all zigzag SWNTs ($\mathbf{k} \| \mathbf{K}_1$), $\mathcal{M}_{ep}^{R,TO} = 0$, while $\mathcal{M}_{ep}^{R,LO}$ has a maximum value.[9] The Θ_R vs θ for SWNTs with the same family number p is shown in Fig. 1(d). For the TO phonon mode, the $\mathcal{M}_{ep}^{R}$ for the SWNT with a similar θ increases with decreasing d_t because of the diameter dependence in the circumferential direction[12] as shown in Fig. 1(b). In a previous paper,[9] we pointed out the importance of the angle ϕ between the SWNT axis and the phonon eigenvector for the LO and TO phonons for the el-ph matrix elements.[20] In fact, when we consider ϕ, then Eq. (4) is modified by

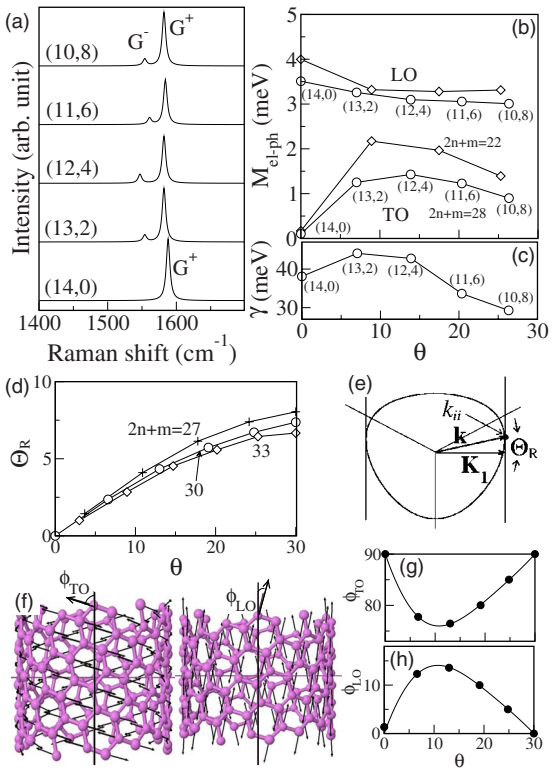

FIG. 1. (Color online) (a) The G-band spectra for S-SWNTs with the same family number $p = 2n+m = 28$. (b) el-ph matrix elements $\mathcal{M}_{ep}^{R}$ vs chiral angle θ for the LO and TO phonons and for two different family numbers (22 and 28). (c) γ vs θ for members of family $p = 28$. (d) Plot of Θ_R vs θ for three $2n+m$ families of M-SWNTs. (e) The angle Θ_R to the cutting line for the polar coordinate of a $\mathbf{k}$ vector at the van Hove singular point. (f) The angle ϕ between the tube axis and the phonon eigenvector direction for a (12,6) SWNT. The calculated angles ϕ vs θ for (g) TO and (h) LO phonons fitted by the function given in the text.

$$\langle e(\mathbf{k}), \omega_{LO}|\mathcal{H}_{ep}|e(\mathbf{k})\rangle = gu\cos[\Theta_R(\mathbf{k}) + \phi],$$

$$\langle e(\mathbf{k}), \omega_{TO}|\mathcal{H}_{ep}|e(\mathbf{k})\rangle = -gu\sin[\Theta_R(\mathbf{k}) + \phi]. \quad (5)$$

Figures 1(f) and 1(g) show that the calculated angle ϕ changes smoothly as function of θ. The sum $\phi_{LO} + \phi_{TO}$ for a general chiral angle θ always becomes $\pi/2$ because of symmetry. The angle ϕ vs θ for the LO and TO phonons can be fitted by the chiral angle dependence $(A + B\theta + C\theta^2)\sin(6\theta)$, where A, B, and C are fitting parameters and θ is the chiral angle in units of degrees (°). For ϕ_{LO}, $A = 26.9$, $B = -76.3$, and $C = 84.5$. For ϕ_{TO}, $A = -26.7$, $B = 75.4$, and $C = -83.2$. This ϕ dependence should be taken into account when carrying out Raman spectral calculations.

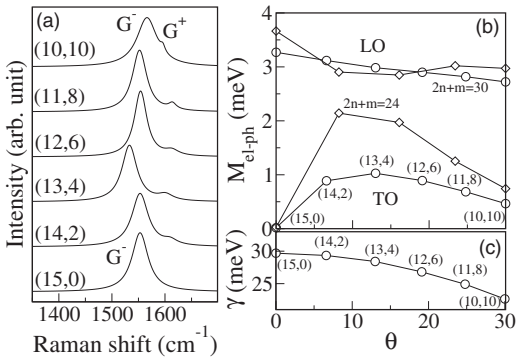

FIG. 2. (a) The *G*-band spectra of M-SWNTs with the same family number $p=30$ and $E_F=0$. (b) el-ph matrix elements vs θ for the LO and TO phonons and for two different family numbers. Open circles indicate the $\mathcal{M}_{ep}$ values for the family number $p=30$. (c) γ vs θ for members of $p=30$.

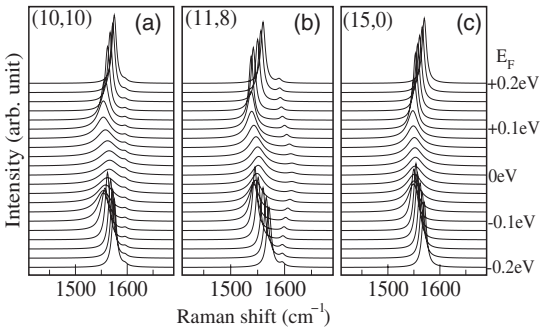

FIG. 3. The *G*-band spectra for three M-SWNTs with different chiral angles taken by changing the Fermi energy from $E_F=-0.2$ to 0.2 eV. (a) (10,10). (b) (11,8). (c) (15,0).

Figure 2(a) shows the calculated Raman spectra for the *G* band of M-SWNTs with family number $p=30$ and $E_F=0$. The E_L and γ [see Fig. 2(c)] are taken from E_{11}^M for each (n,m) SWNT. The G^- peak intensity is larger than that of the G^+ peak because the $G^-(G^+)$ peak corresponds to the LO (TO) phonon due to the LO phonon softening in which $\mathcal{M}_{ep}^{R,LO} > \mathcal{M}_{ep}^{R,TO}$ for any θ value, as shown in Fig. 2(b). The relative intensities of the two peaks, G^+ and G^-, are affected by the Raman spectral width, which relates to the phonon lifetime, Γ. For the (10,10) armchair SWNT, the G^+(TO) peak width is significantly smaller than those of the G^-(LO) peak and of the G^+ peaks for the other chiral tubes. Therefore, the G^+ peak intensity of the (10,10) tube becomes large compared with the other chiral SWNTs, even though the $\mathcal{M}_{ep}^{R,TO}$ for the armchair tube has a smaller value than for the other chiral tubes. It is noted that the Raman peak intensity is determined by the large $\mathcal{M}_{ep}^{R}$ and small Γ values, which is the reason why the G^+/G^- spectra show an irregular behavior as a function of (n,m). For the (15,0) zigzag SWNT, only the G^+ peak appears because $\mathcal{M}_{ep}^{R,TO}$ vanishes for zigzag nanotubes as seen in Eq. (4). The other chiral tubes in this family, (11,8), (12,6), (13,4), and (14,2), show various intermediate intensity ratios. In Fig. 2(c), we show that γ decreases monotonically with increasing θ. Because of the small difference of the γ and of the el-ph coupling for the LO phonon as compared to that of the TO for a change in θ, the G^- peak intensity does not show a large change for the different chiral SWNTs. The G^+/G^- spectral feature depends on θ but is more sensitive to the E_F position, especially for M-SWNTs.

Figure 3(a) shows the calculated *G*-band spectra for various E_F at 300 K for a (10,10) armchair SWNT. Here we did not consider the changes in the C-C bond or the E_{ii} transition energy by doping with electron or holes. In the experiment, the E_{ii} is slightly changed with changing E_F, which results in an off-resonance situation for a fixed laser excitation energy E_L. Here, $+E_F$ $(-E_F)$ corresponds to electron (hole) doping. When E_F is changed from $E_F=0$, the G^- peak shows a frequency shift and a sharpening of the spectral width, while the G^+ peak does not give any change in frequency or width. Sasaki *et al.*[9] reported that an intermediate electron-hole pair state contributes to the softening of the LO phonon but does not couple to the TO phonon for armchair SWNTs. For the chiral M-SWNT (11,8) as shown in Fig. 3(b), both the LO and TO phonons couple to the intermediate electron-hole pair state, which is excited by a lower-energy phonon. The TO phonon becomes harder for $E_F=0$ eV since the intermediate state of an electron-hole pair for $E<\hbar\omega_{TO}$ contributes to a TO phonon hardening.[9] In the case of the (15,0) SWNT, the G^+ peak always vanishes because of a vanishing $\mathcal{M}_{ep}^{R,TO}$, as discussed above.

The matrix element $\mathcal{M}_{ep}^{KA}$ for the KA effect in Eq. (3) is given by[9]

$$\mathcal{M}_{ep}^{KA,LO} \equiv \langle eh(\mathbf{k})|\mathcal{H}_{ep}|\omega_{LO}\rangle = igu \sin\Theta_{KA}(\mathbf{k}),$$

$$\mathcal{M}_{ep}^{KA,TO} \equiv \langle eh(\mathbf{k})|\mathcal{H}_{ep}|\omega_{TO}\rangle = -igu \cos\Theta_{KA}(\mathbf{k}), \quad (6)$$

where $\Theta_{KA}(\mathbf{k})$ is defined by the angle between the $\mathbf{k}$ point taken on a cutting line for two-linear metallic subbands and the nanotube circumferential direction of a unit vector, $\mathbf{K}_1$. For the armchair nanotube, the cutting line for the two-linear metallic bands lies on the nanotube axis direction unit vector, and then Θ_{KA} is $\pi/2$ $(-\pi/2)$, which gives a vanishing $\mathcal{M}_{ep}^{KA,TO}$. For a chiral nanotube, Θ_{KA} is not zero since the cutting line for the two-linear metallic bands deviates from the *K* point due to the curvature effect, and then the KA effect appears in both the LO and TO modes. For the zigzag M-SWNT (15,0), only the G^+ peak related to the TO phonon appears since the el-ph matrix element for the Raman-scattering process has a zero value, as shown in Fig. 2(b). Thus, we only measure a LO phonon softening experimentally, even though a TO phonon hardening was expected theoretically.

The calculated *G*-band Raman spectra vs E_F can be directly compared with the experimental *G*-band Raman spectra, which are obtained for electrochemically doped individual SWNTs, as seen in Fig. 4. Here we assume $\Delta E_F = 0.3\Delta V_g$ according to Ref. 21. The experimental Raman spectra are shown in Figs. 4(a), 4(c), and 4(e), and the calculated Raman spectra are shown in Figs. 4(b), 4(d), and 4(f). In Fig. 4(a), the experimental Raman spectra show only a LO phonon softening, and a TO phonon frequency shift does not occur. As mentioned above, for the armchair SWNT, the TO phonon frequency shift does not appear and

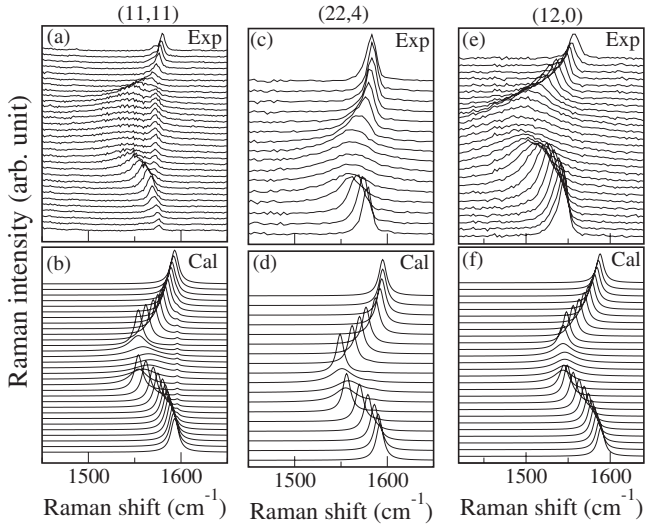

FIG. 4. (a), (c), and (e) Experimental *G*-band Raman spectra, which are given by the electrochemical doping effect. (a) $V_g=1.5$ to -1.5 V. (c) $V_g=1.9$ to -1.3 V. (e) $V_g=1.3$ to -1.3 V. (b), (d), and (f) Calculated *G*-band Raman spectra taken by changing the Fermi energy E_F (b) 0.45 to -0.45 eV, (d) 0.60 to -0.42 eV, and (f) 0.39 to -0.39 eV. (a) and (b) (11,11), (c) and (d) (22,4), and (e) and (f) (12,0).

only LO phonon softening appears. Therefore we can predict that Fig. 4(a) shows an armchair-type behavior by changing the gate voltage. The RBM peak for these experimental Raman spectra appears at 161 cm^{-1} with $E_L=1.72$ eV. Then we can select the possible (n,m) values by using a simple tight-binding model with $\gamma_0=2.9$ eV for simplicity and by using the relation between RBM frequency and diameter, $\omega_{RBM}(\text{cm}^{-1})=248/d_t(\text{nm})$. Thus, the possible (n,m) values are (19,1), (18,3), (14,8), and (11,11). If our prediction is correct, Fig. 4(a) can be assigned to an (11,11) armchair SWNT. Figures 4(c) and 4(e) are assigned as chiral (22,4) and zigzag (12,0) SWNTs, respectively, from the possible (n,m) values, {(21,6),(22,4),(23,2)} and {(10,4),(11,2),(12,0)}. For the chiral M-SWNTs, not only the LO phonon softening but also the TO phonon hardening appear in the *G*-band Raman spectra vs E_F in the calculation. However, in Fig. 4, the TO peak is too small to be seen on this intensity scale. Figure 4(e) shows that a zigzag SWNT has only the G^- peak and thus only the LO phonon softening appears by changing E_F, experimentally. Brown *et al.*[22] and others[23,24] pointed out that asymmetric line-shape appears in the G^--band Raman spectrum for metallic tubes, which is related to the Fano resonance (Breit-Wigner-Fano) lines. However it should be pointed out that the present calculation does not consider the interaction of the phonon with the continuum state, which will be studied in a future work.

In conclusion, the *G*-band resonance Raman spectra are given as a function of chiral angle, metallicity, and E_F position. A comprehensive study of the Raman spectra can be understood by considering the el-ph matrix elements, the broadening factor, and the KA effect, which give unique Raman spectra for M-SWNTs. Thus, the Raman spectra of the *G* band will be useful especially for a single SWNT transistor in which the E_F is changed by the gate voltage. Not only the (n,m) assignment but also the E_F position can be obtained from contactless Raman measurements.

R.S. acknowledges a Grant-in-Aid from MEXT, Japan (Grant No. 20241023). The MIT authors acknowledge support under NSF (Grant No. DMR 07-04197). M.K. acknowledges support from the Czech Ministry of Education, Youth and Sports (Contracts No. LC-510 and No. ME09060).

[1] M. S. Dresselhaus *et al.*, Phys. Rep. **409**, 47 (2005).
[2] J. Jiang *et al.*, Phys. Rev. B **71**, 205420 (2005).
[3] K. Ishikawa and T. Ando, J. Phys. Soc. Jpn. **75**, 084713 (2006).
[4] V. N. Popov and P. Lambin, Phys. Rev. B **73**, 085407 (2006).
[5] N. Caudal *et al.*, Phys. Rev. B **75**, 115423 (2007).
[6] A. Das *et al.*, Phys. Rev. Lett. **99**, 136803 (2007).
[7] K. T. Nguyen *et al.*, Phys. Rev. Lett. **98**, 145504 (2007).
[8] H. Farhat *et al.*, Phys. Rev. Lett. **99**, 145506 (2007).
[9] K. Sasaki *et al.*, Phys. Rev. B **77**, 245441 (2008).
[10] Z. Yu and L. E. Brus, J. Phys. Chem. B **105**, 6831 (2001).
[11] R. Saito *et al.*, Phys. Rev. B **64**, 085312 (2001).
[12] J. Jiang *et al.*, Phys. Rev. B **72**, 235408 (2005).
[13] J. Kürti and H. Kuzmany, Phys. Rev. B **44**, 597 (1991).
[14] A. Grüneis *et al.*, Phys. Rev. B **67**, 165402 (2003).
[15] J. Jiang *et al.*, Carbon **42**, 3169 (2004).
[16] Ge. G. Samsonidze *et al.*, Appl. Phys. Lett. **85**, 5703 (2004).
[17] D. Porezag *et al.*, Phys. Rev. B **51**, 12947 (1995).
[18] J. S. Park *et al.*, Phys. Rev. B **74**, 165414 (2006).
[19] R. Saito *et al.*, Phys. Rev. B **72**, 153413 (2005).
[20] S. Reich *et al.*, Phys. Rev. B **64**, 195416 (2001).
[21] K. Sasaki *et al.*, Phys. Rev. B **78**, 235405 (2008).
[22] S. D. M. Brown *et al.*, Phys. Rev. B **63**, 155414 (2001).
[23] Y. Wu *et al.*, Phys. Rev. Lett. **99**, 027402 (2007).
[24] A. W. Bushmaker *et al.*, Nano Lett. **9**, 607 (2009).